NACA

RESEARCH MEMORANDUM

SUMMARY OF ROCKET-MODEL TESTS AT ZERO LIFT OF AN ARROW-WING MISSILE CONFIGURATION FROM MACH NUMBERS OF 0.9 TO 1.8

By Richard G. Arbic and Warren Gillespie, Jr.

Langley Aeronautical Laboratory
Langley Field, Va.

NATIONAL ADVISORY COMMITTEE
FOR AERONAUTICS

WASHINGTON

January 14, 1954

NACA RM L53J02

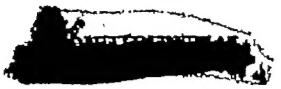

NATIONAL ADVISORY COMMITTEE FOR AERONAUTICS

RESEARCH MEMORANDUM

SUMMARY OF ROCKET-MODEL TESTS AT ZERO LIFT OF AN ARROW-WING MISSILE CONFIGURATION FROM MACH NUMBERS OF 0.9 TO 1.8

By Richard G. Arbic and Warren Gillespie, Jr.

SUMMARY

Flight tests were conducted between Mach numbers of 0.9 to 1.8 over a Reynolds number range from 9×10^6 to 30×10^6 to determine the zero-lift drag and some rolling-effectiveness characteristics of a proposed long-range, supersonic, ground-to-ground missile. The missile configuration had an arrow-shaped wing plan form and was tested with both a small and a large body. The wing had 67.5° leading-edge sweep, 15° trailing-edge sweep, and a modified NACA 0004 airfoil section. The proposed missile had no horizontal tail, but had wing trailing-edge elevons which served a dual purpose as elevators and ailerons. The ratio of body frontal area to wing plan-form area was 0.0127 for the small-body configuration and 0.0330 for the large-body configuration.

Five 1/14-scale models were flown permitting determination of the zero-lift drag of the basic small-body configuration, the incremental drag due to the large body, the incremental drag resulting from a blunt wing trailing edge, the wing-plus-interference drag, and some rolling-effectiveness data.

Results indicated that the proposed missile had low supersonic zero-lift drag, the maximum zero-lift drag coefficients being 0.0125 and 0.0155 at a Mach number of 1.03 for the small- and large-body configurations, respectively. The effect of a blunt wing trailing edge, obtained by cutting off 10 percent of the wing chord, was to increase the zero-lift drag by 13 to 21 percent. Wing-plus-interference drag accounted for 78 percent of the total drag at Mach number 0.9 and 70 percent at Mach number 1.5 for the small-body configuration. The ailerons produced positive rolling effectiveness for the wing stiffness of the test models and the dynamic pressures of the test.

INTRODUCTION

The Langley Pilotless Aircraft Research Division has investigated the zero-lift drag and some rolling-effectiveness characteristics of a proposed long-range, supersonic, ground-to-ground missile configuration. The proposed missile had a wing, body, and vertical tail, but had no horizontal tail. Longitudinal control was to be achieved by means of wing-trailing-edge elevons which served as both elevators and ailerons. The arrow-shaped wing had an aspect ratio of 1.86 with 67.5° leading-edge sweep, 15° trailing-edge sweep, and a modified NACA 0004 airfoil section. The wing was mounted on a small body of maximum cross-sectional area equal to 1.27 percent of the total wing area. A large-body version of the missile had a body of maximum cross-sectional area equal to 3.30 percent of the wing area. An alternate wing design investigated had a blunt trailing edge obtained by cutting off 10 percent of the basic wing chord.

This paper summarizes the results of the rocket-model tests of the proposed missile configuration. Five 1/14-scale models were flown permitting determination of the zero-lift drag of the basic small- and large-body configurations, the incremental drag due to the large body, the drag penalty due to the blunt wing trailing edge, the wing-plus-interference drag, and some rolling-effectiveness data. A portion of the data presented herein was previously reported in the rocket-model tests of reference 1. Flight tests were conducted at the Langley Pilotless Aircraft Research Station at Wallops Island, Va.

SYMBOLS

A	model cross-sectional area perpendicular to fuselage center line, sq ft
a_l	longitudinal acceleration, ft/sec^2
a_n	normal acceleration, ft/sec^2
b	wing span, ft
c	airfoil chord, ft
C_D	drag coefficient based on total wing area of 5.61 sq ft, $-Wa_l/32.2qS$

[redacted]

ΔC_D	incremental drag coefficient based on total wing area of 5.61 sq ft
C_N	normal-force coefficient based on total wing area, $Wa_n/32.2qS$
h	thickness of wing trailing edge, ft
l	length of model fuselage, ft
M	Mach number
p	rolling velocity, radians/sec
q	dynamic pressure, lb/sq ft
R	Reynolds number based on wing mean aerodynamic chord of 2.31 ft
r_{equiv}	equivalent body radius, ft
S	total wing area including portion within the fuselage, 5.61 sq ft
S_a	aileron area, sq ft
t	wing maximum thickness, ft
V	velocity, ft/sec
W	model weight, lb
x	distance from nose of fuselage to any station on the fuselage, ft
$\frac{pb}{2V}/\delta$	rolling-effectiveness parameter, per degree
δ	average elevon deflection, deg

MODELS

The five models tested are shown in figure 1, and the body and airfoil ordinates are listed in table I. The basic arrow wing had an aspect ratio of 1.86, 67.5° leading-edge sweep, 15° trailing-edge sweep, and a

[redacted]

modified NACA 0004 airfoil section. The model vertical tails had 0° sweep of the 50-percent-chord line and had the same exposed plan form but differed slightly in airfoil section, as shown in figure 1. Models 1, 2, 3, and 4 had a small body of fineness ratio 15.5 and a maximum cross-sectional area located at approximately 30 percent of the body length and equal to 1.27 percent of the total wing area. The wing of model 2 was modified by cutting off the last 10 percent of the chord resulting in a trailing-edge sweep of 25.8° and forming a blunt trailing edge with a base area equal to 0.85 percent of the wing area. In addition, model 2 had a booster-coupling support strut approximately two-thirds the size of that shown on model 5 in figure 1 and similarly located. The wing of model 3 had the trailing-edge ailerons deflected to roll the model. One aileron was deflected 3.05° up and the other 2.40° down resulting in an average deflection of 2.73°. Model 4 did not have a wing but had horizontal stabilizing fins. Model 5 had a large body of fineness ratio 14.9 and a maximum cross-sectional area located at approximately 50 percent of the body length and equal to 3.30 percent of the total wing area. The models were of wood and metal construction.

Photographs of the small- and large-body models are shown in figures 2 and 3. The cross-sectional-area distribution along the model center line and the equivalent body radius for these two configurations are presented in figure 4. The plot of equivalent body radius shows the body shape that would result if all the cross-sectional area at a station were put into a body of revolution. The equivalent body for the large-body configuration has a higher fineness ratio and less severe boattail than does the small body.

INSTRUMENTATION AND TESTS

Instrumentation for all models except model 4 consisted of a 2-channel telemeter transmitting longitudinal and normal accelerations. Model 4 had no instrumentation; drag for this model was obtained solely from differentiation of Doppler determined radar velocity. For the instrumented models, drag was obtained, when possible, from both radar and longitudinal accelerometer data. Rolling velocity was obtained from the polarized telemeter antenna signal used in conjunction with the spinsonde receiving equipment. The position of the model in space and the atmospheric conditions were obtained, respectively, by means of an NACA modified SCR 584 radar tracking unit and by a radiosonde balloon released at the time of firing. An external booster rocket motor was used to accelerate the models to their peak velocity. Aerodynamic data were obtained during model coasting flight following separation from the booster.

[redacted]

The range of Reynolds number (based on the wing mean aerodynamic chord of 2.31 feet) for the tests is shown in figure 5. Reynolds numbers for all tests varied within the range from approximately 9×10^6 at Mach number 0.9 to 30×10^6 at Mach number 1.8.

ACCURACY OF DATA

The accuracy of the data, based on instrumentation ranges and experience in rocket-model testing, is estimated to be as follows:

Mach number	± 0.010
C_D (at M = 0.9)	± 0.0010
C_D (at M = 1.5)	± 0.0006
C_N (at M = 0.9)	± 0.016
C_N (at M = 1.5)	± 0.005
$\frac{pb}{2V}/\delta$ (at all values of M)	± 0.0012

RESULTS AND DISCUSSION

Results obtained from the tests are presented in figures 6 to 11. Curves of trim normal-force coefficient, rolling effectiveness, and a time history of the roll-model flight are presented in addition to the zero-lift—drag data. The effect on the drag of the slightly different vertical-tail sections and of the booster coupling support struts was negligible and is, therefore, not considered in the discussion of the drag for the various models.

Longitudinal Trim

Trim normal-force coefficient for the winged models (1, 2, 3, and 5) is shown as a function of Mach number in figure 6. The data show that the models trimmed to essentially zero normal force but indicate a slightly positive normal force in the transonic region. The normal accelerometer of the roll model registered negative normal force above Mach number 1.0 (see fig. 11) but the normal-force coefficient obtained for this model agreed with that for the nonrolling models when corrected for centrifugal force due to normal-accelerometer displacement from the roll axis. Near Mach number 1.0, the roll model experienced some instability in yaw due to rolling. This instability will be discussed more fully in a later section.

[redacted]

Drag

Figure 7 presents the variation with Mach number of the zero-lift drag coefficient for each of the models tested. The fine grid has been retained in this figure for greater ease of reading the drag coefficients.

The drag coefficients for the various models are compared in figure 8(a). The small- and large-body configurations are seen to have low supersonic zero-lift drag coefficients. The drag is a maximum near Mach number 1.03 and decreases gradually with Mach number. The basic small-body configuration (model 1) has a subsonic drag coefficient of 0.008 increasing to a maximum of 0.0125 and decreasing to 0.010 at Mach number 1.8. Addition of the large body results in a subsonic drag coefficient of 0.009 with a maximum value of 0.0155 decreasing to 0.0131 at Mach number 1.4. The drag coefficients for the basic small-body model and the roll model show essentially no differences, an indication that the average aileron deflection of 2.73° resulted in no measurable drag increase. The curve shown for "model 4 without horizontal fins" was determined by subtracting the known drag coefficient for the horizontal fins, obtained as explained in reference 1, from that of the fin-stabilized body model. The curve shown is, therefore, the variation of drag coefficient for the small body with vertical tail except for interference-drag effects which could not be accounted for.

The blunt-trailing-edge model (model 2) is seen in figure 8(a) to have appreciably higher drag than does the basic small-body configuration. The incremental drag due to the blunt trailing edge is shown in figure 8(b) and represents an increase of 20 percent at Mach number 0.95, 21 percent at Mach number 1.03, and 13 percent at Mach number 1.5 over the drag of the basic small-body configuration. It is also shown that the drag contribution due to the blunt trailing edge is a minimum near Mach number 0.98 and a maximum near Mach number 1.10. The circular symbol at Mach number 1.5 in figure 8(b) was obtained by using base-pressure data from reference 2 for a wing with a blunt trailing edge and with $t/c = 0.05$ and $h/t = 0.25$. For the blunt wing of the present test, $t/c = 0.04$ and $h/t = 0.21$. Addition to the flight data of the estimated skin-friction drag for the cut-off portion of the blunt wing results in close agreement at Mach number 1.5 with the data from reference 2. The base drag on the blunt trailing edge is large, probably as a result of the nearly two-dimensional character of the flow over the wing. Reference 3 indicates that the base drag of a body of revolution with the same base area as that of the wing would be approximately 50 percent of that due to wing-trailing-edge bluntness at Mach number 1.5.

Figure 8(c) presents the drag increase of the large-body model over that of the basic small-body configuration. The increase is a maximum just below Mach number 1.0. It should be realized that this curve and also the curve of figure 8(b) could be altered appreciably in this region

[redacted]

due to a possible Mach number error of 0.01. The drag increment of figure 8(c) represents an increase of 13 percent at Mach number 0.90, 24 percent at 1.03, and 17 percent at 1.4.

The wing-plus-interference drag coefficient presented in figure 8(d) was obtained by subtracting the body-plus-vertical-tail drag coefficient from that of the basic small-body configuration and shows that the wing-plus-interference drag accounted for approximately 78 percent of the total drag at Mach number 0.9 and 70 percent at Mach number 1.5.

Rolling Effectiveness

Rolling-effectiveness data obtained from the flight of the roll model are shown in figure 9(a) between Mach numbers 1.0 and 1.4, and dynamic pressures for the test are presented in figure 9(b). The δ used in the rolling-effectiveness parameter $\frac{pb}{2V}/\delta$ was the average aileron deflection (2.73°). The rolling-effectiveness parameter varied uniformly from approximately 0.02 at Mach number 1.02 to 0.0065 at Mach number 1.39. There is no evidence of aileron reversal for the Mach number range covered. The rolling effectiveness of similar ailerons on a 60° delta wing from the rocket-model tests of reference 4 is shown for comparison. The more rapid decrease of rolling effectiveness with increasing Mach number for the present configuration could be partially due to a more flexible wing construction and thinner wing section for the present-test model since the dynamic pressures of the two tests were comparable.

Some indication as to the flexibility of the roll-model wing is shown in figure 10. This figure shows the deflection of the wing at various spanwise stations due to a torque of 20 foot-pounds applied at a distance of 16 inches from the model center line. The applied torque is seen to result in camber of the wing in a manner to reduce the rolling effectiveness. The aileron load would have a similar cambering effect.

Instability Due to Roll

Figure 11 presents a time history of longitudinal acceleration, normal acceleration, roll velocity, and Mach number during flight of the roll model. The model appears to have experienced some degree of instability below Mach number 1.0. This is thought to be a result of roll as described in reference 5 since the nonrolling models had no difficulty. Calculations of the undamped pitching and yawing natural frequencies for the model indicated that the yawing natural frequency was of the order of 40 radians per second and that this was approximately one-half the pitching natural frequency. Although no rolling velocity was obtained after approximately 8.2 seconds of flight, it is interesting to note that instability is

indicated when the rolling velocity reached a value of approximately 40 radians per second and that this condition would produce instability in yaw since, as stated in reference 5, instability occurs when the rolling frequency exceeds the lower of the pitching and yawing natural frequencies. It should be pointed out that although a condition of instability due to roll appears to have occurred for the 1/14-scale model of the present test, an analysis would be required to indicate whether the full-scale missile would suffer from this condition.

SUMMARY OF RESULTS

Results of free-flight rocket-model tests of the arrow-wing missile configuration are as follows:

1. The basic small- and large-body configurations had low supersonic drag. The small-body configuration with body-to-wing area ratio of 0.0127 had a subsonic drag coefficient of 0.0080 increasing to a maximum of 0.0125 at Mach number 1.03 and decreasing to 0.010 at Mach number 1.80. Increasing the body-to-wing area ratio to 0.033 resulted in an increase in drag coefficient of 13 percent at Mach number 0.90, 24 percent at Mach number 1.03, and 17 percent at Mach number 1.40.

2. The effect of the blunt wing trailing edge, obtained by cutting off 10 percent of the basic wing chord, was to increase the zero-lift drag coefficient by approximately 20 percent at Mach number 0.95, 21 percent at Mach number 1.03, and 13 percent at Mach number 1.50.

3. For the basic small-body configuration, the wing-plus-interference drag accounted for approximately 78 percent of the total drag at Mach number 0.9 and 70 percent at Mach number 1.5.

4. The trailing-edge constant-chord ailerons resulted in positive rolling effectiveness (i.e., no aileron reversal) for the Mach number range covered and for the dynamic pressures and wing flexibility of the test. The rolling-effectiveness parameter $\frac{pb}{2V}/\delta$ had a value of 0.020 at Mach number 1.02 and 0.0065 at Mach number 1.39.

Langley Aeronautical Laboratory,
National Advisory Committee for Aeronautics,
Langley Field, Va., September 22, 1953.

[redacted]

REFERENCES

1. Gillespie, Warren, Jr., and Arbic, Richard G.: Large-Scale Flight Measurements of Zero-Lift Drag at Mach Numbers From 0.90 to 1.95 of an Arrow Wing in Combination With a Small Body. NACA RM L50K28a, 1951.

2. Chapman, Dean R., Wimbrow, William R., and Kester, Robert H.: Experimental Investigation of Base Pressure on Blunt-Trailing-Edge Wings at Supersonic Velocities. NACA Rep. 1109, 1952. (Supersedes NACA TN 2611.)

3. Seiff, Alvin, Sandahl, Carl A., Chapman, Dean R., Perkins, E. W., and Gowen, F. E.: Aerodynamic Characteristics of Bodies at Supersonic Speeds. A Collection of Three Papers. NACA RM A51J25, 1951.

4. Sandahl, Carl A., and Strass, H. Kurt: Comparative Tests of the Rolling Effectiveness of Constant-Chord, Full-Delta, and Half-Delta Ailerons on Delta Wings at Transonic and Supersonic Speeds. NACA RM L9J26, 1949.

5. Phillips, William H.: Effect of Steady Rolling on Longitudinal and Directional Stability. NACA TN 1627, 1948.

[redacted]

TABLE I.- BODY AND WING AIRFOIL-SECTION ORDINATES

Airfoil-section ordinates modified NACA 0004	
Station, percent c	Upper and lower ordinates, percent c
0	0
1.25	.6325
2.50	.8660
5.00	1.1900
7.50	1.4000
10.00	1.5550
15.00	1.7780
20.00	1.9100
25.00	1.9780
30.00	2.0000
40.00	1.9310
Straight line	Straight line
75.00	1.0420
Straight line	Straight line
100.00	0
L.E. radius: 0.178	

Small-body ordinates	
Station, in. from nose	Radius, in.
0	0
1.000	.259
2.000	.491
3.000	.703
4.000	.893
7.375	1.386
10.375	1.654
13.375	1.785
15.375	1.808
18.375	1.808
20.000	1.806
23.000	1.787
26.000	1.748
29.000	1.690
32.000	1.615
35.000	1.526
38.500	1.406
42.500	1.251
46.500	1.081
49.078	.965
50.078	.909
51.078	.837
52.078	.742
53.078	.618
54.078	.457
55.078	.253
56.078	0

Large-body ordinates	
Station, in. from nose	Radius, in.
0	0
.885	.203
3.885	.742
6.885	1.150
9.885	1.480
12.885	1.756
15.885	1.990
18.885	2.189
24.885	2.500
30.885	2.713
36.885	2.839
42.885	2.881
45.885	2.870
48.885	2.839
51.885	2.787
54.885	2.713
57.885	2.618
60.885	2.500
63.885	2.358
66.885	2.189
69.885	1.990
72.885	1.756
75.885	1.480
78.885	1.150
81.885	.742
84.885	.203
85.770	0

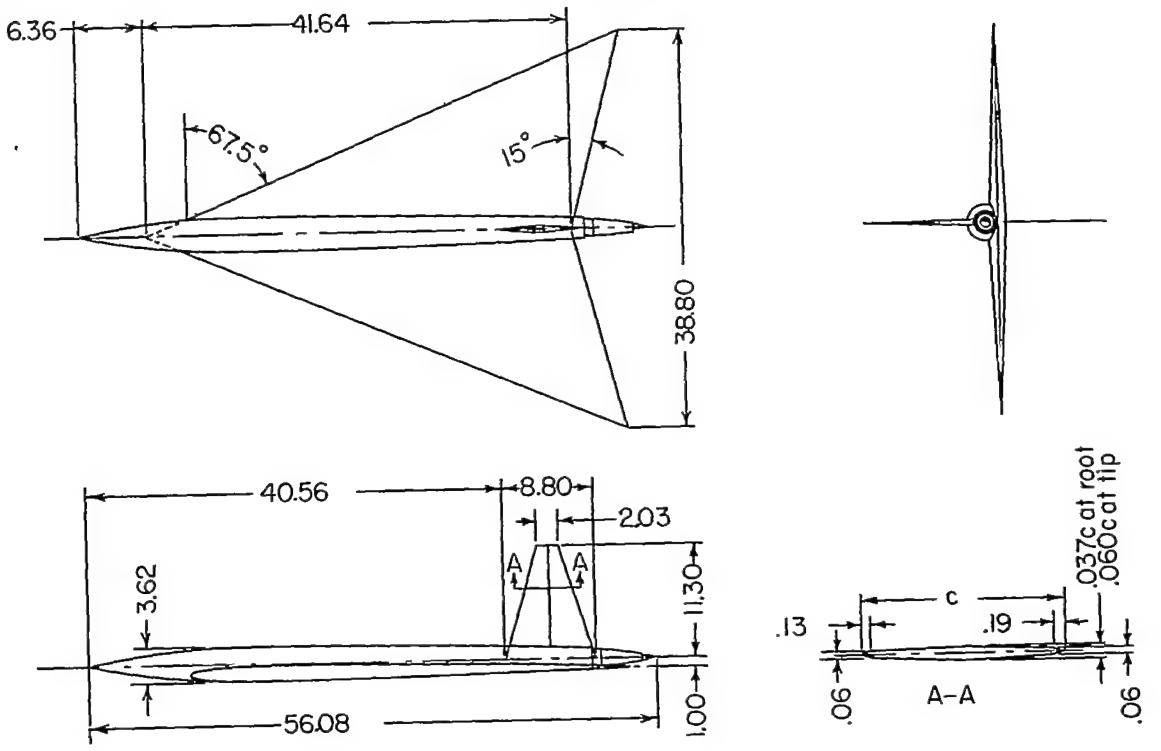

Model 1: Basic small-body drag model.

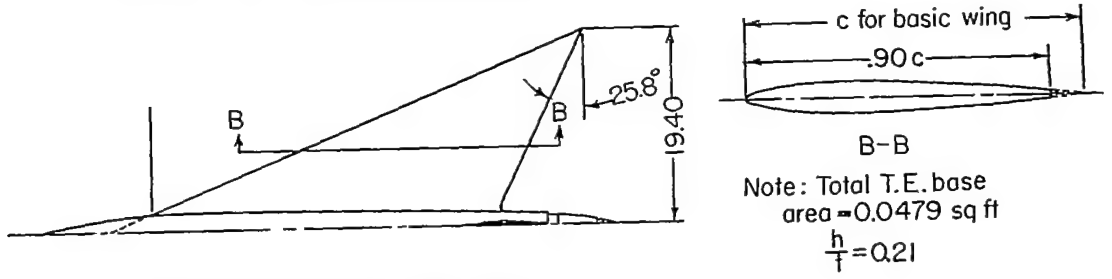

Model 2: Blunt-trailing-edge model.

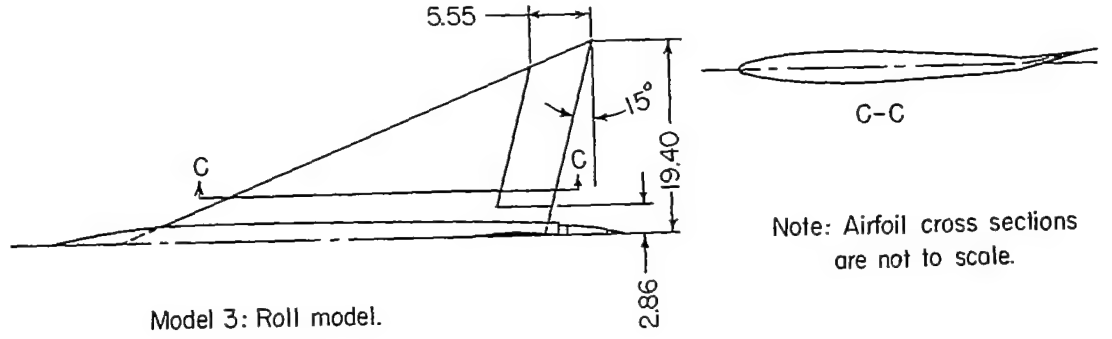

Model 3: Roll model.

Figure 1.- General arrangement of test models. All dimensions are in inches.

[redacted]

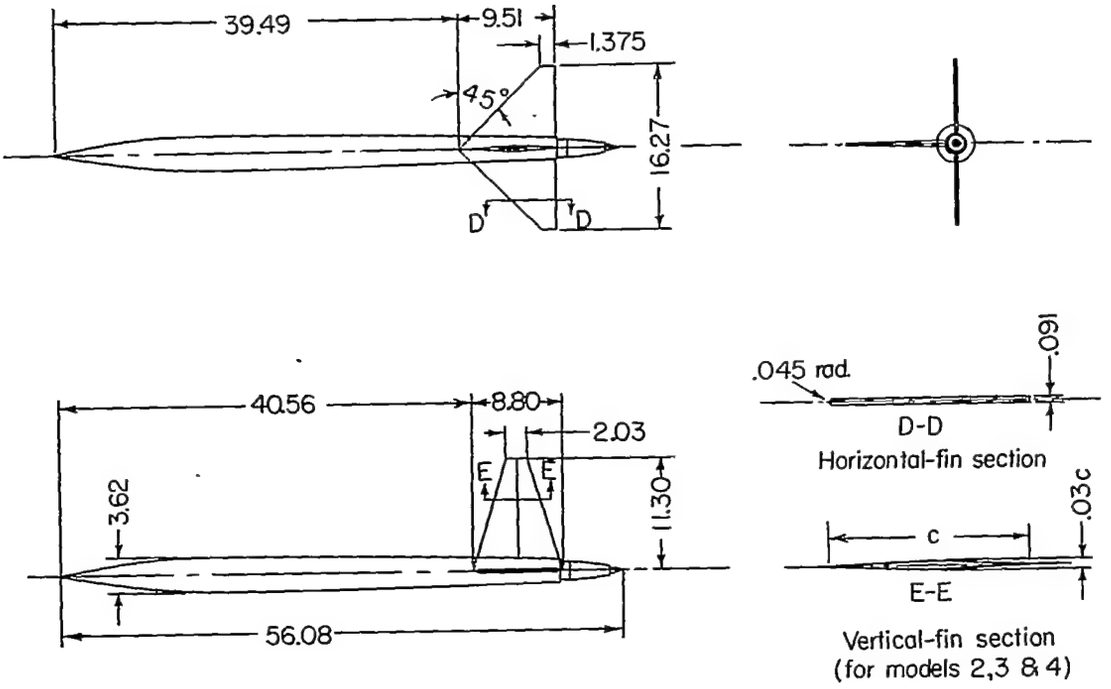

Model 4: Body-fin model.

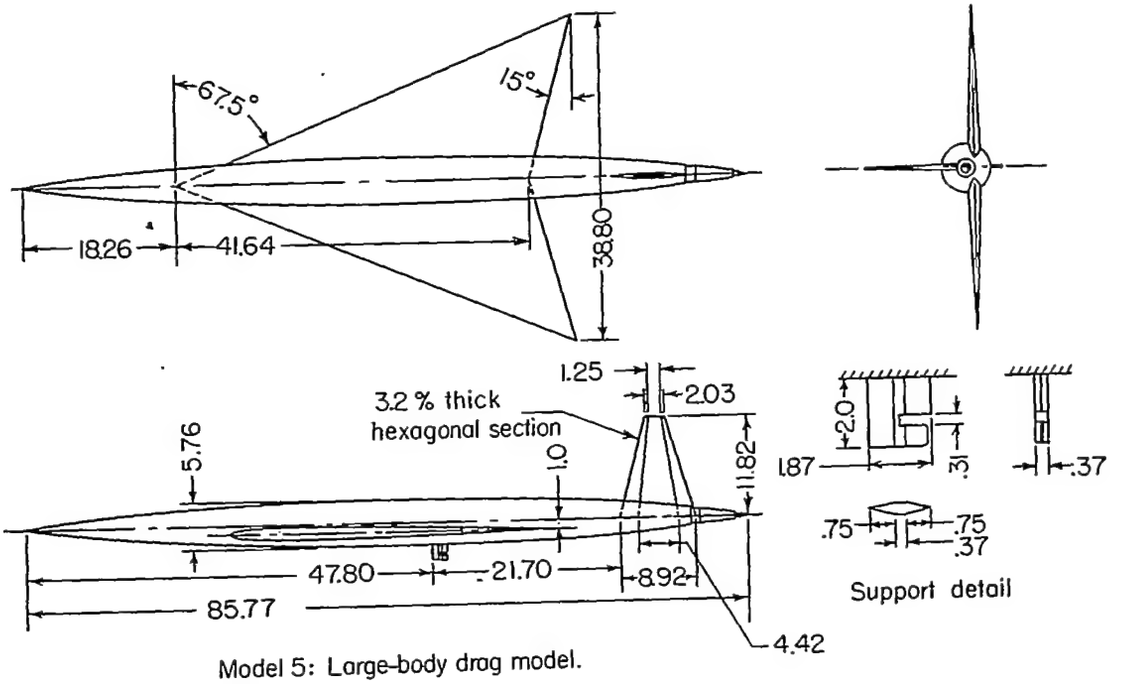

Model 5: Large-body drag model.

Figure 1.- Concluded.

[redacted]

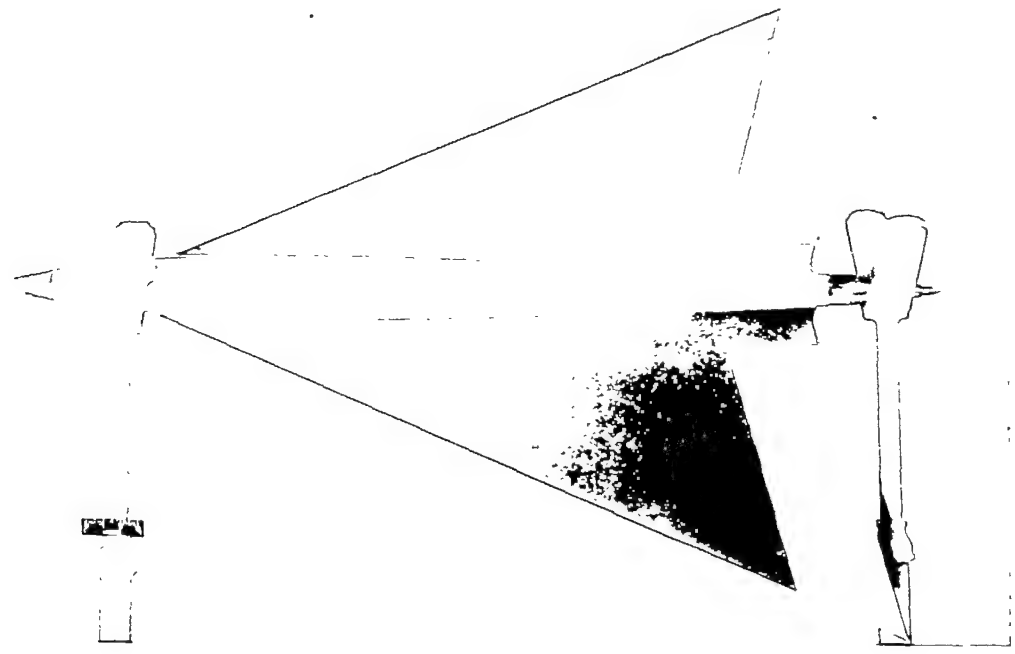

L-71696.1

(a) Top view.

L-65632.1

(b) Side view.

Figure 2.- Photograph of basic small-body configuration.

[redacted]

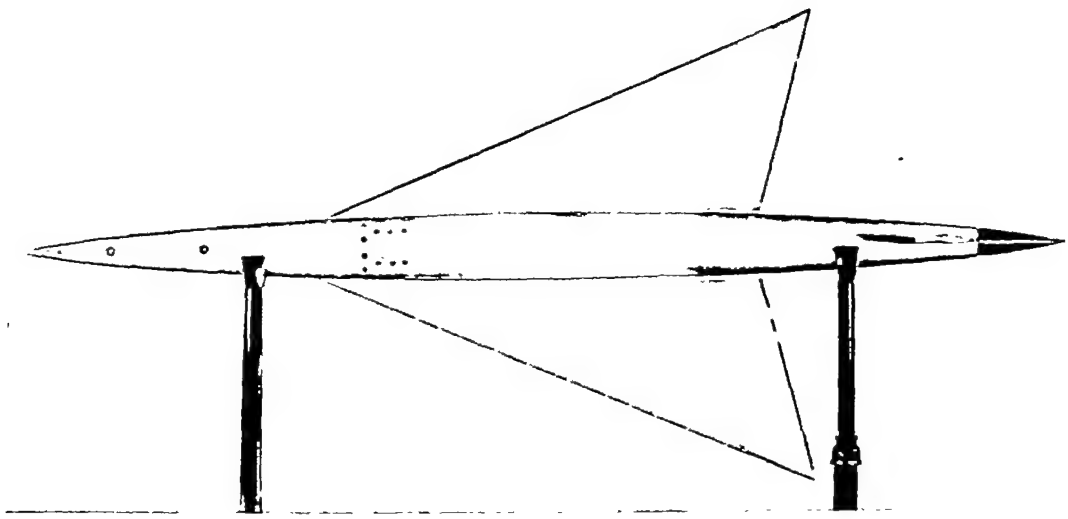

L-78426.1

(a) Top view.

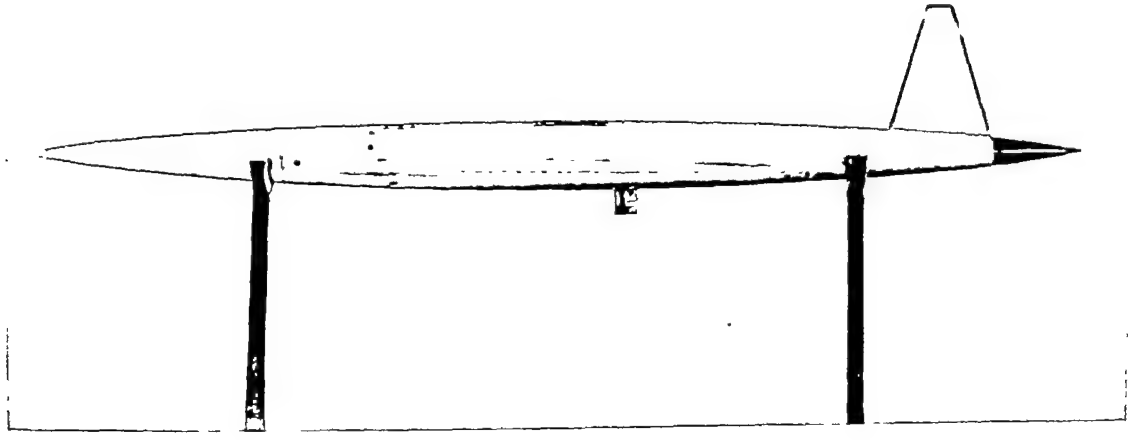

L-78425.1

(b) Side view.

Figure 3.- Photograph of large-body configuration.

[redacted]

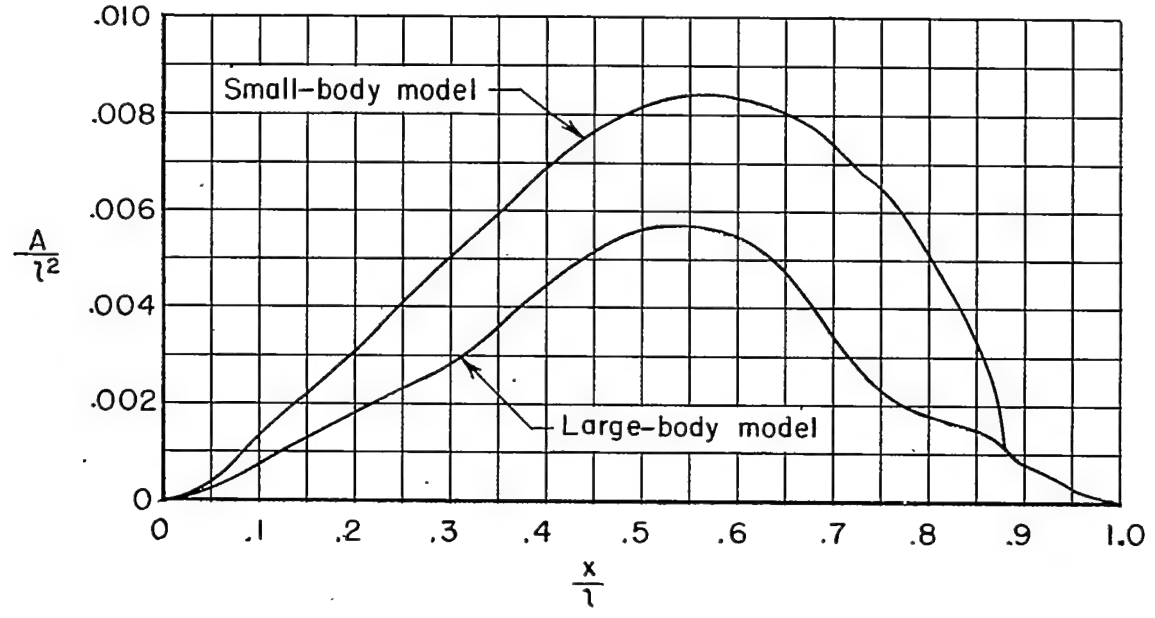

(a) Area distribution.

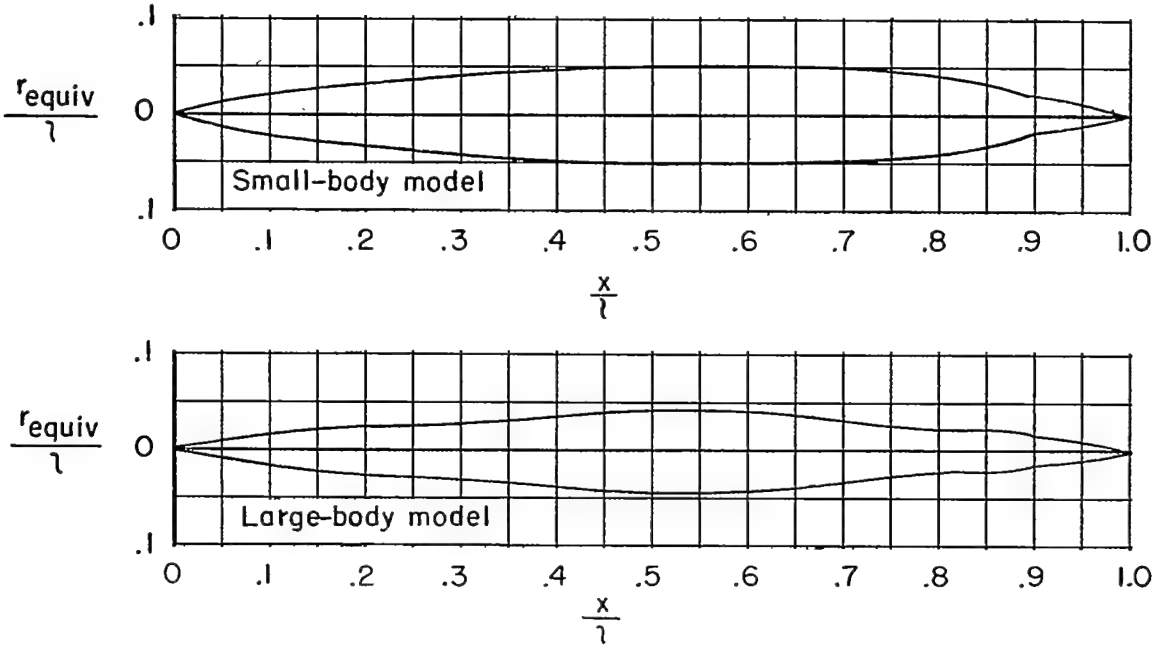

(b) Equivalent radius.

Figure 4.- Nondimensional cross-sectional area distribution and equivalent radius for the basic small- and large-body models (models 1 and 5) as a function of nondimensional body length.

[redacted]

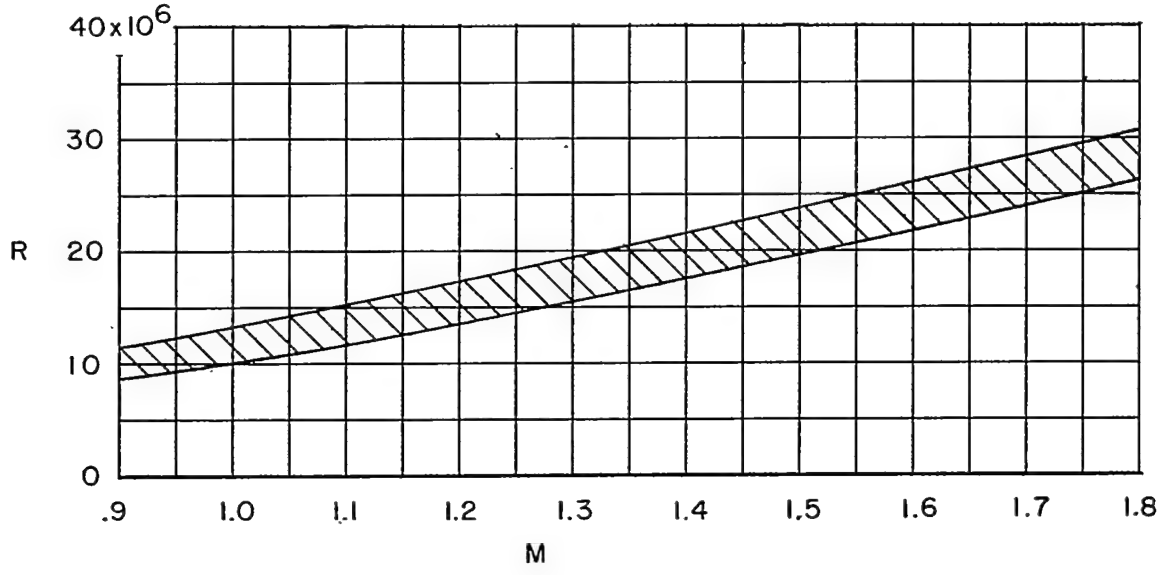

Figure 5.- Range of Reynolds number based on the wing mean aerodynamic chord for the models tested.

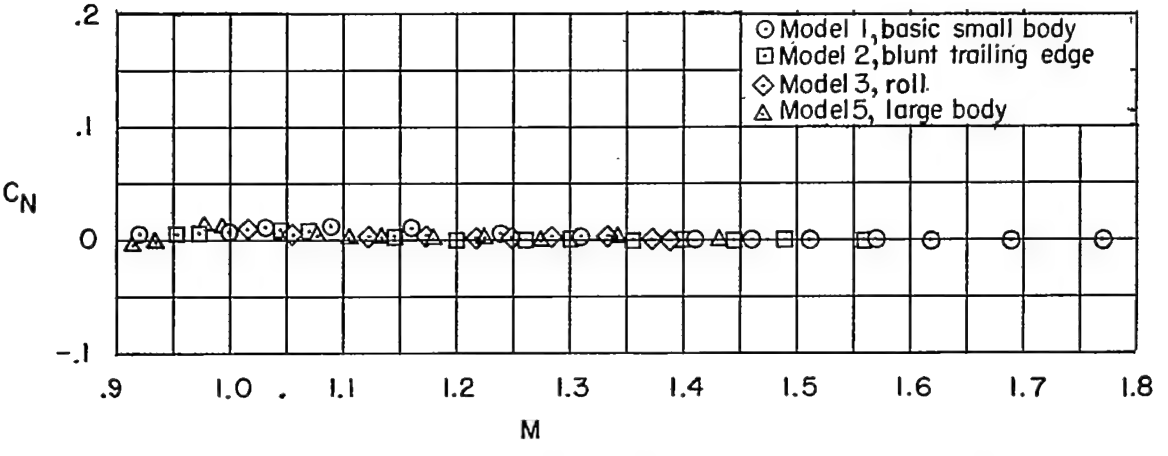

Figure 6.- Variation of normal-force coefficient with Mach number.

[redacted]

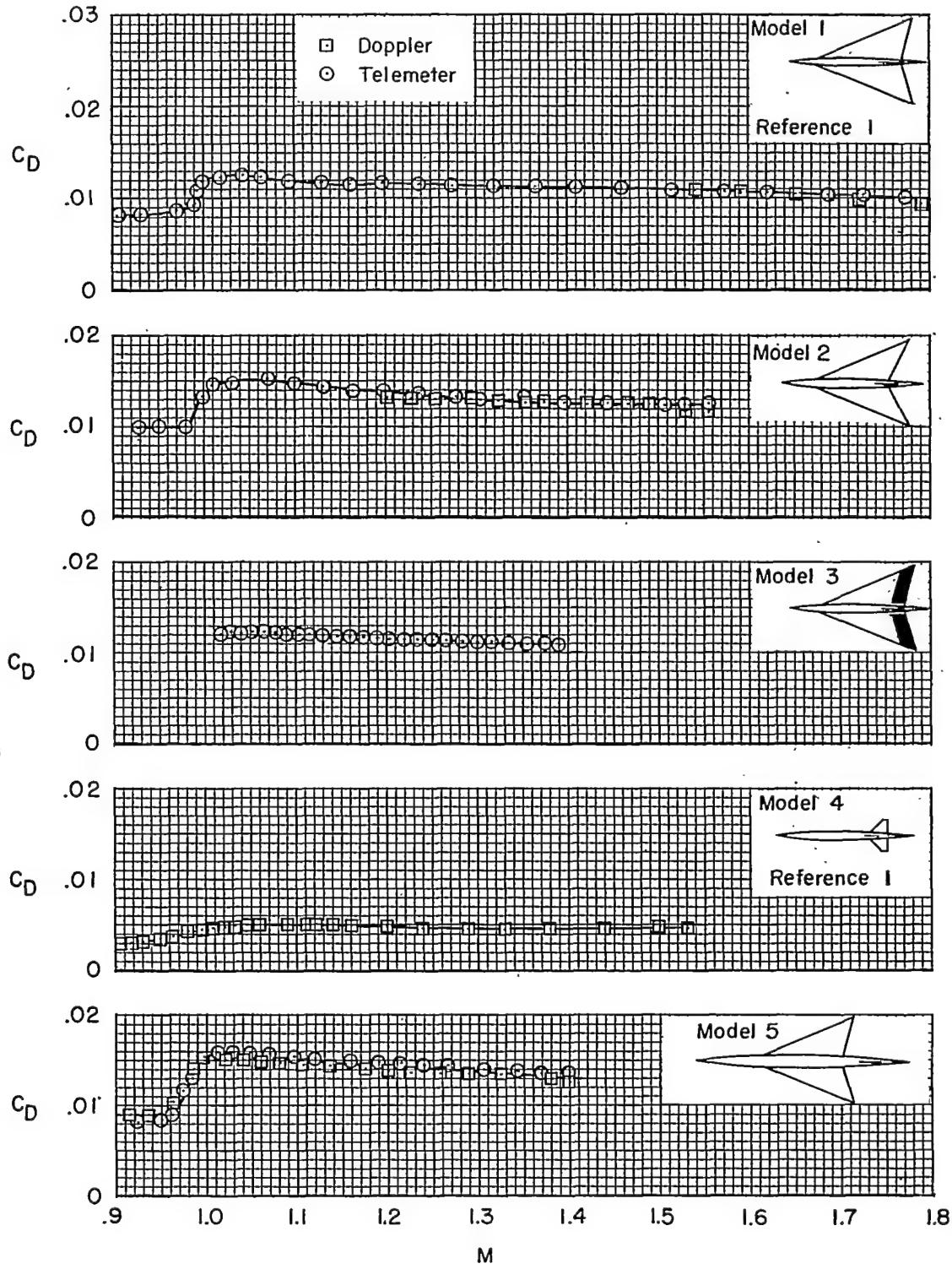

Figure 7.- Zero-lift drag coefficient as a function of Mach number for the various models.

[redacted]

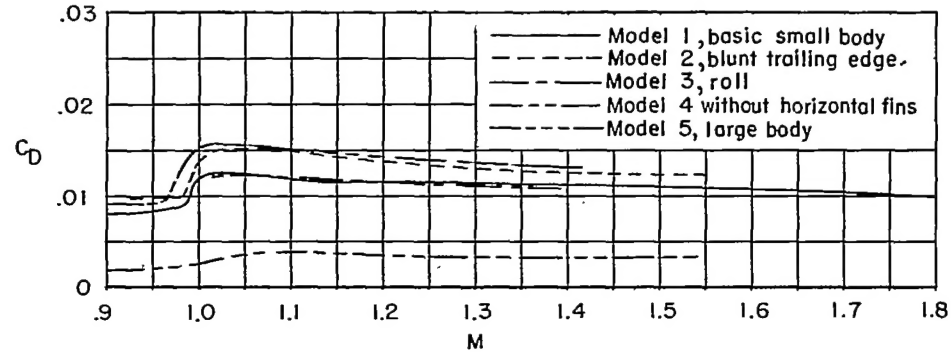

(a) Comparison of the model drag coefficients.

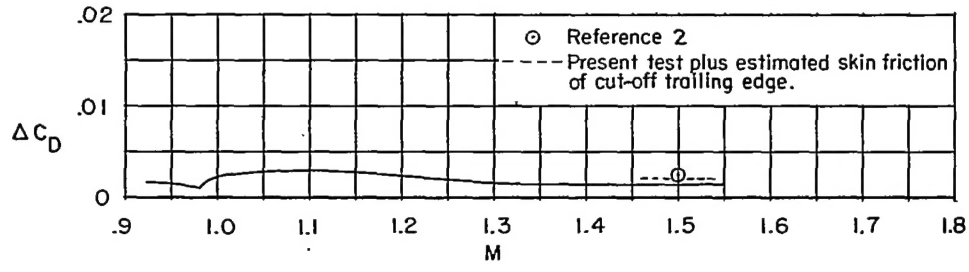

(b) Contribution of the blunt trailing edge.

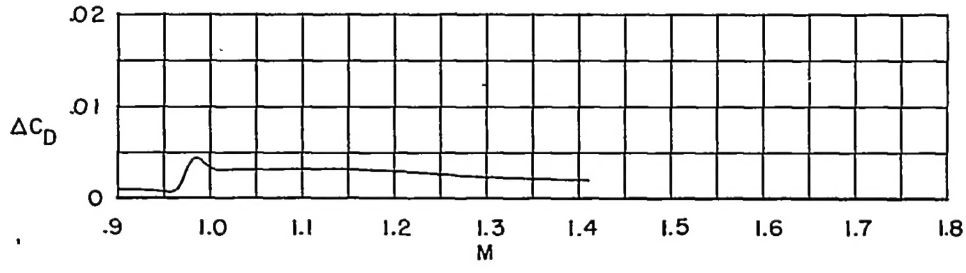

(c) Contribution due to increased body size.

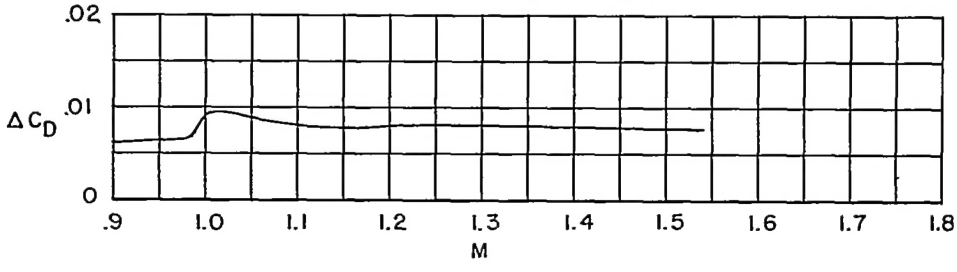

(d) Contribution of the wing with interference.

Figure 8.- Comparison of model drag coefficients and variation with Mach number of the incremental drag coefficients due to trailing-edge bluntness, addition of the large body, and to the wing with interference.

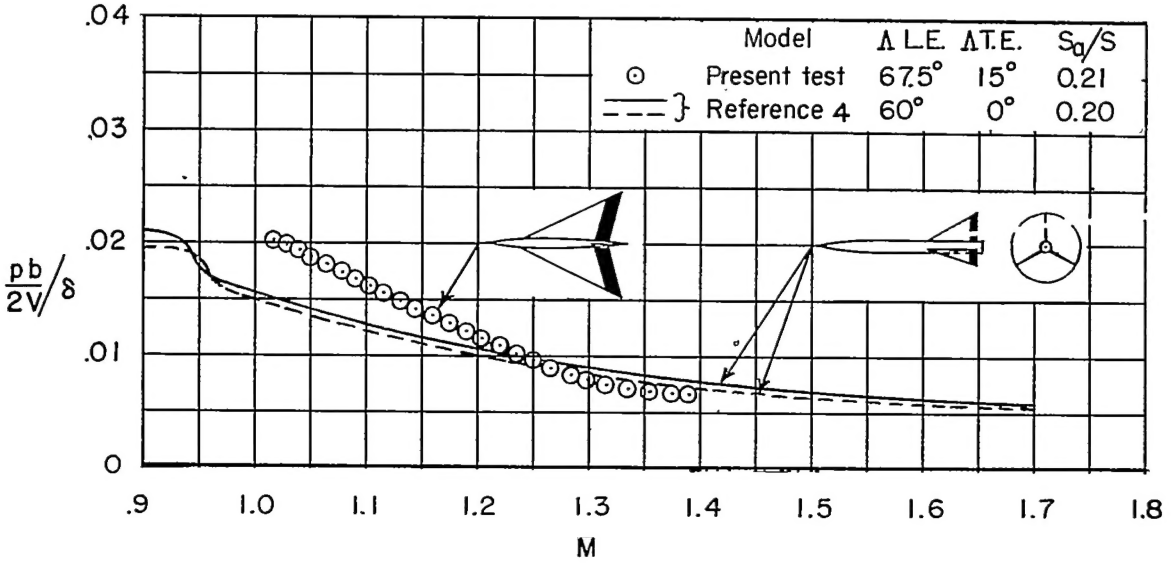

(a) Rolling effectiveness.

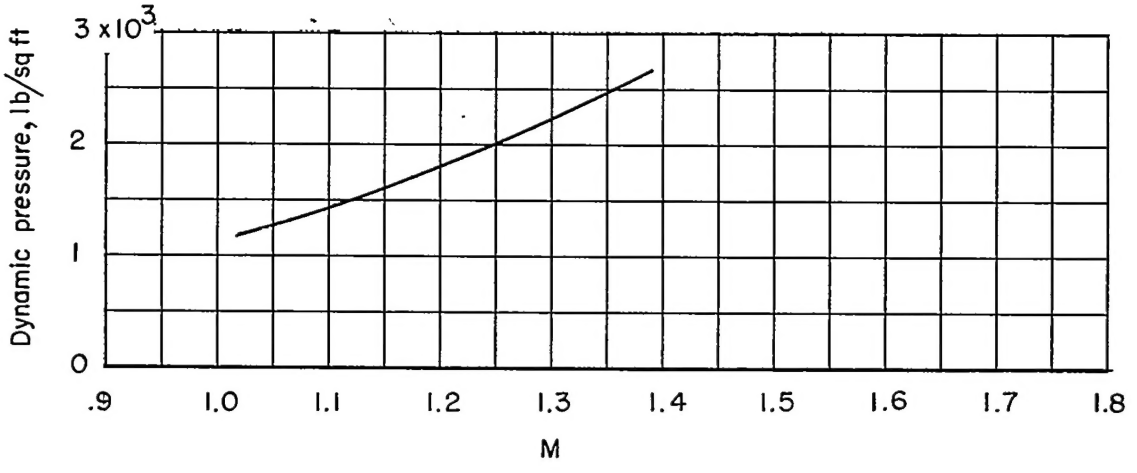

(b) Dynamic pressure.

Figure 9.- Rolling effectiveness and dynamic pressure as a function of Mach number.

[redacted]

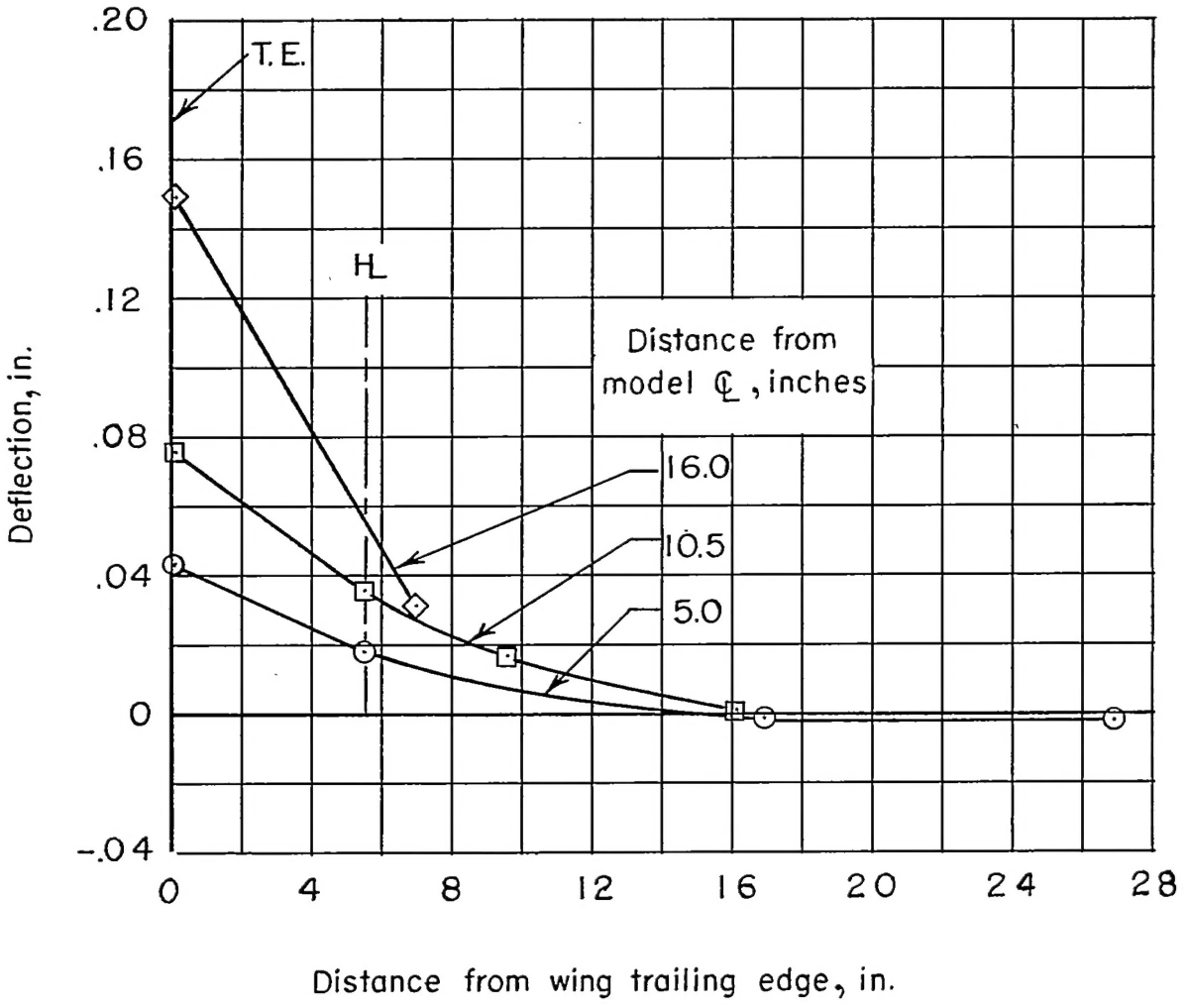

Figure 10.- Deflection of the roll-model wing due to a torque of 20 foot-pounds applied at station 16 inches from the model center line.

[redacted]

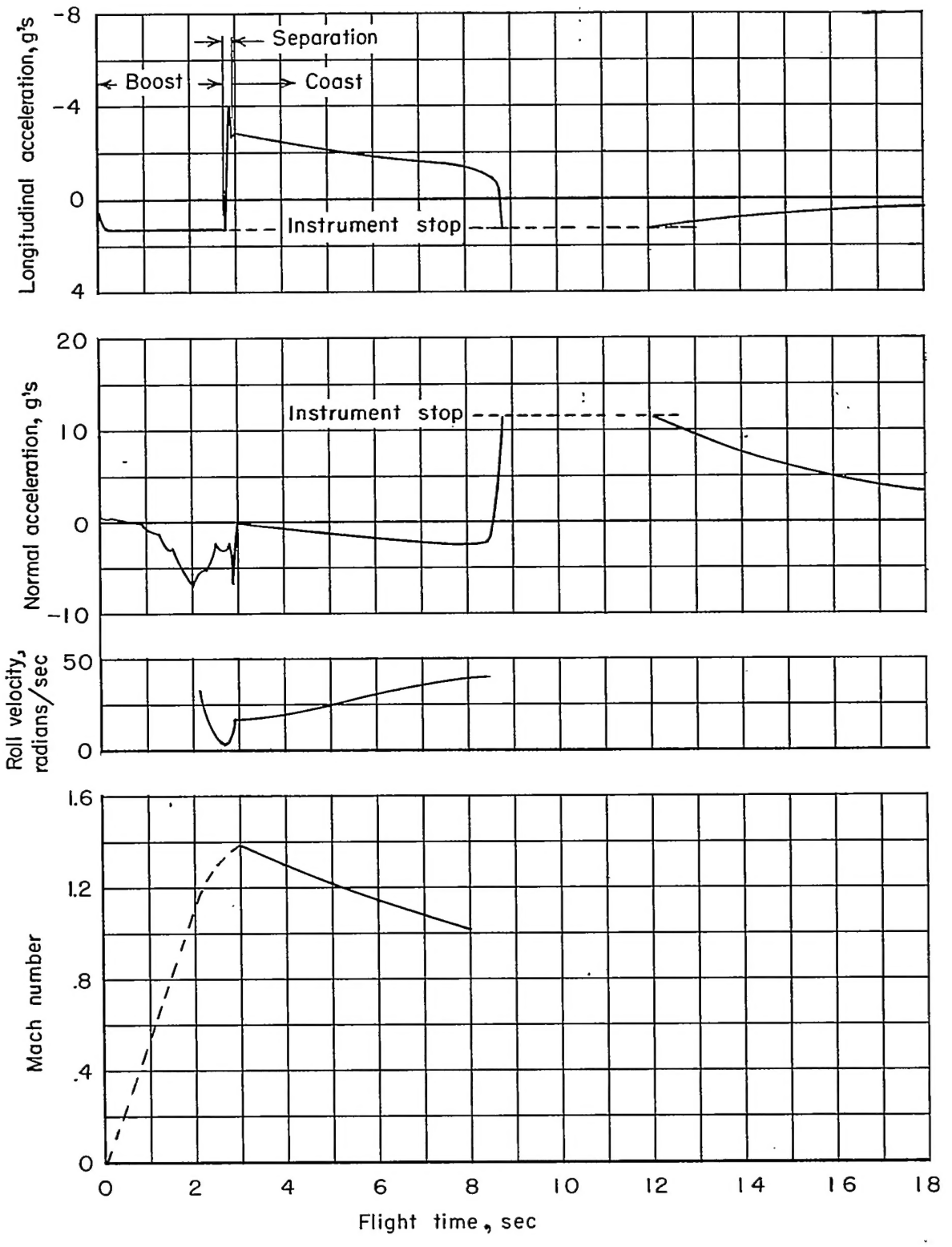

Figure 11.- Time history of flight of the roll model showing the instability due to roll experienced in the transonic region.

[redacted]

NACA-Langley - 1-14-54 - 325